Physics Letters B 811 (2020) 135865

Contents lists available at ScienceDirect

Physics Letters B

www.elsevier.com/locate/physletb

Symmetry energy effect on emissions of light particles in coincidence with fast fission

Qianghua Wu [a], Fenhai Guan [a], Xinyue Diao [a], Yijie Wang [a], Yingxun Zhang [b], Zhuxia Li [b], Xizhen Wu [b], Artur Dobrowolski [c], Krzysztof Pomorski [c], Zhigang Xiao [a,*]

[a] Department of Physics and Collaborative Innovation Center of Quantum Matter, Tsinghua University, Beijing 100084, China
[b] China Institute of Atomic Energy, P.O. Box 275(18), Beijing 102413, China
[c] Uniwersytet Marii Curie Skłodowskiej, Katedra Fizyki Teoretycznej, Lublin 20031, Poland

ARTICLE INFO

Article history:
Received 9 March 2020
Received in revised form 28 August 2020
Accepted 6 October 2020
Available online 15 October 2020
Editor: W. Haxton

Keywords:
Symmetry energy
Fast fission
Heavy ion reactions

ABSTRACT

The emission of light particles in coincidence with fast fission in near peripheral reactions of ^{40}Ar+^{197}Au at 30 MeV/u beam energy has been studied by using the Improved Quantum Molecular Dynamics Model (ImQMD). It is demonstrated that in the symmetrical fast fission of the heavy target-like fragment (TLF), the emission of the coalescence-invariant neutrons (CIN) is enhanced particularly at large angles in comparison to that in the events without fission. Due to the enhanced CIN emission and the accumulation of the isospin effect in the long-time process, the yield ratio of the CIN to the coalescence-invariant protons (CIP) in the fission events exhibits significant dependence on the symmetry energy $E_{\rm sym}(\rho)$ varying with density. Considering that the large angle neutrons are experimentally advantageous to measure for the lower flying velocity and lower multiplicity, we emphasize that the yield ratio $R_{\rm CINP}$ at large angles in the fast fission events can be used as a novel probe of the nuclear symmetry energy at sub-saturation densities.

1. Introduction

Nuclear symmetry energy varying with density $E_{\rm sym}(\rho)$ is crucial not only for understanding nuclear structures and nuclear reactions, particularly those induced by neutron-rich radioactive nuclei but also for understanding many stellar processes of dense objects in the astrophysical environment. In astrophysics, the unique neutron star merging event GW170817 stimulates enormous studies on constraining the nuclear symmetry energy in the density range of 1-2ρ_0 where ρ_0 is the saturation density [1–7]. In nuclear physics, great progress has been made to constrain symmetry energy through various probes from subsaturation density to about 2ρ_0 [8–21], yet its accurate density dependence has not been achieved. Above saturation density $\rho > \rho_0$, the constraint of $E_{\rm sym}(\rho)$ from various heavy-ion data analysis is still controversial [22,23]. At $\rho \approx \rho_0$ where the situation is better, there is still large room to reduce the uncertainty of the slope parameter of $E_{\rm sym}(\rho)$. Currently, large efforts are taken both experimentally and theoretically to improve the accuracy of constraining nuclear symmetry energy, for instance, by introducing the Bayesian analysis [4,24], checking the correlation among multi observables [25], allocating the source of a discrepancy of different transport models [26] and searching for new observable sensitive to it [27–29].

As a potential candidate in searching new probes of $E_{\rm sym}(\rho)$, fast fission refers to the fission process for which the fission barrier vanishes because of the high excitation energy and large angular momentum, which are usually achieved in heavy-ion reactions at about 10 MeV/u beam energy and beyond [30–33]. Unlike statistical fission, fast fission has a shorter time scale, a wider distribution of fragment mass and a larger asymmetry of fission fragment mass [34–38]. Meanwhile, the study shows that the relative velocity of fission fragments satisfies the Viola systematics [38,39]. The light particle emissions in coincidence with this process can be used to build a nuclear clock to measure the fission time scale insensitive reportedly to the mass or charge of the light particles [40,41].

It has been suggested for the following reasons that the light particles emitted from the fast fission events carry the information of symmetry energy. First, from the overlap region of the projectile and the target in the collision, usually referred as the projectile-target neck region, the emission of particles with enhanced neutron richness in mid-rapidity is observed as a favored probe of $E_{\rm sym}(\rho)$ [42–45] in accordance with early transport model predictions [44]. Then, if the heavy TLF, similarly as the projectile-like fragments (PLF) in reverse kinetics, further undergoes fast fission

* Corresponding author.
E-mail address: xiaozg@tsinghua.edu.cn (Z. Xiao).

https://doi.org/10.1016/j.physletb.2020.135865

Table 1
Interaction parameters in ImQMD simulation [53].

α (MeV)	β (MeV)	γ	g_{sur} (MeV· fm^2)	$g_{sur,iso}$ (MeV· fm^2)	$g_{\rho\tau}$ (MeV)	η	ρ_0 (fm^{-3})
−207	138	7/6	18.0	−1.6	14.0	5/3	0.1650

following the collision, the second neck is formed during the rupture. The presence of the neck will possibly have several favorable facets to visualize the symmetry energy effects. i) the neck develops and experiences again a low-density and neutron-rich stage, ii) the surface is extended because the highly excited TLF is split to two smaller fragments favoring the emission of particles from the surface, and iii) the fission fragments possess usually smaller equilibrated N/Z than the fissioning TLF so that more neutrons are emitted as either free nucleons or bounded in clusters. Recently, the fission of the PLF has been observed in correlation with the rotation angle of the fissioning axis representing the time, and the isospin migration via the neck has been demonstrated from the evolution of the N/Z of the lighter fission fragments as a function of the rotation angle [37,46]. Reporting that the isospin drift mechanism persists to a very late stage of the reactions and isospin effect is accumulated during the whole process [42,43], it is then a natural idea to identify a probe to $E_{\rm sym}(\rho)$ using the light particles associated with the fast fission.

However, making use of the fast fission events to constrain $E_{\rm sym}(\rho)$ is not straightforward because the emitted light particles in the fission events originate from many sources, including intermediate velocity (IV) source, the PLF, the TLF and the neck region associated with the fission of the latter. Particularly the mixing of the origins from the IV and the real neck of the fissioning TLF, both of which are characterized by enhanced neutron richness, makes the analysis even more complicated. Moving source analysis can in principle differentiate various sources but with the risk that the fitting parameters which are too many are correlated. Thanks to the running of many 4π detectors covering very large to the whole phase space in the center of mass system around the world [47–51], it is quite possible to observe the fine effect of enhancement of neutron richness in the light particle emissions of the fissioning TLF.

The motivation of this letter is to study the effect of the occurrence of the fission on the emission of light particles in heavy-ion reactions at Fermi energies using the transport model. Instead of localizing the neck area in coordinate space in simulations, which is anyway unachievable in an experiment, we emphasize on the comparison of the spectra between the events with and without undergoing fast fission. As long as the fast fission process has been simulated by the ImQMD transport model as demonstrated in our previous publication [52], we further conduct the simulation and analysis of the light particle spectra by varying form of the nuclear symmetry energy $E_{\rm sym}(\rho)$. The experimental feasibility is taken into account when we present the results to propose a new probe to constrain $E_{\rm sym}(\rho)$ near saturation density. The letter is organized as follows. Section 2 is a brief introduction to the ImQMD model. In section 3, the simulation results and discussions are presented. The summary is given in section 4.

2. The ImQMD model

We adopted the ImQMD model (Version ImQMD05 [56]) to simulate the fast fissions events in ^{40}Ar+^{197}Au reactions at Fermi energies. Basically, the QMD-type model, which has been widely used to describe various large-amplitude motion modes in nuclear collisions with success, traces the N-body behavior of the nucleons of the projectile and the target by solving the canonical motion equations in a semi-classic way. The quantum effect was taken into account in the treatment of every single nucleon, which is represented by Gaussian wave packets as

$$\phi_j(\mathbf{r}) = (2\pi\sigma_r^2)^{-3/4} exp[-(\frac{\mathbf{r}-\mathbf{r}_j}{2\sigma_r})^2 + i\frac{\mathbf{r}\cdot\mathbf{p}_j}{\hbar}] , \tag{1}$$

where $\mathbf{r}_j$ and $\mathbf{p}_j$ are the coordinate and momentum vectors of the jth nucleon. The wave packet width in coordinate space is $\sigma_r = \sigma_0 + \sigma_1 A^{1/3}$ fm, with $\sigma_0 = 0.49$ and $\sigma_1 = 0.16$ in our calculation. The canonical equations describing the evolution of each nucleon are written as

$$\dot{\mathbf{r}}_j = \frac{\partial H}{\partial \mathbf{p}_j}, \dot{\mathbf{p}}_j = -\frac{\partial H}{\partial \mathbf{r}_j} . \tag{2}$$

Here H represents the Hamiltonian containing the kinetic energy and the potential energy. The equations (2) are solved numerically by tracing the propagation of all nucleons in fine time steps in the momentum and coordinate space after the projectile and the target nuclei are randomly initialized. To accumulate sufficient statistics, one has to simulate thousands of collision events with the initialized projectile and target passing the stability test. The mean fields acting on the wave packets are derived from an energy density functional with the potential energy

$$U = U_{\rm loc} + U_{\rm Coul} , \tag{3}$$

where $U_{\rm Coul}$ denotes the Coulomb energy and $U_{\rm loc} = \int V_{\rm loc}(\mathbf{r})d\mathbf{r}$ is the Skyrme potential energy. The nucleonic potential energy density $V_{\rm loc}(\mathbf{r})$ is represented in a local form with

$$V_{\rm loc} = \frac{\alpha}{2}\frac{\rho^2}{\rho_0} + \frac{\beta}{\gamma+1}\frac{\rho^{\gamma+1}}{\rho_0{}^{\gamma}} + \frac{g_{sur}}{2\rho_0}(\nabla\rho)^2 + \frac{g_{sur,iso}}{2\rho_0}\left[\nabla(\rho_n-\rho_p)\right]^2 + \frac{C_s}{2}(\frac{\rho}{\rho_0})^{\gamma_i}\delta^2\rho + g_{\rho\tau}\frac{\rho^{\eta+1}}{\rho_0{}^{\eta}} \tag{4}$$

Here, ρ_n, ρ_p are the neutron and proton densities, respectively. $\delta = (\rho_n - \rho_p)/(\rho_n + \rho_p)$ is the isospin asymmetry. In the Skyrme energy density functional, the spin-orbit term is omitted. As listed in Table 1, except for C_s and γ_i which are varied in the simulation, the parameters of the isoscalar part are taken from the IQ3 set [53]. With this parameter set and applying the technique of phase space constraint [54], the initialized nucleus can keep stable for longer than 2000 fm/c and the charge distribution has been reproduced well in low and intermediate energy heavy ion reactions [55]. Moreover, the IQ3 parameter set has been used to simulate and reproduce the main features of the fast fission process [52].

In the formula (4), the two parameters C_s and γ_i correspond to the symmetry potential coefficient and the power of the density dependence of symmetry potential energy, respectively. Since it is well known that these two parameters are correlated, we conducted the calculation by varying both C_s and γ_i in the range of $36 \le C_s \le 44$ and $0.6 \le \gamma_i \le 1.1$, respectively, in approximate accordance with the wide range constrained currently, to investigate the effect of $E_{\rm sym}(\rho)$ on the particle emissions in heavy ion reactions.

3. Results and discussions

Before surveying the isospin effect on the particle emissions in the fission events, we first investigate the features of the fission of the TLF. After scanning the impact parameter from 1 to 8

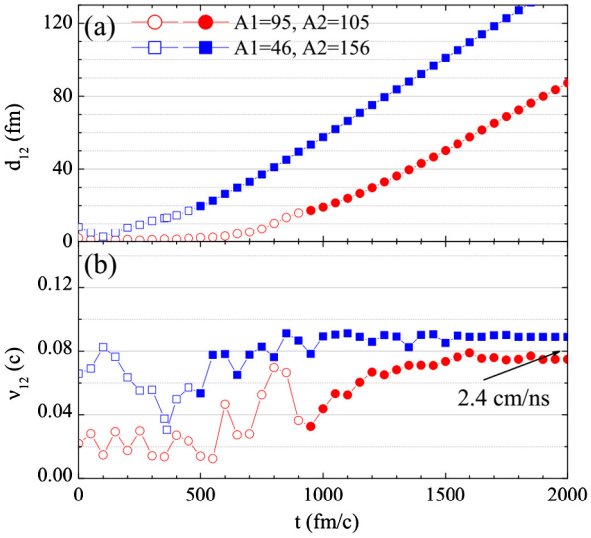

Fig. 1. Evolution of two typical events for symmetrical (red circle) and asymmetrical (blue square) fission, respectively, in 30 MeV/u ^{40}Ar+^{197}Au reactions at $b = 6$ fm. Panel (a) and (b) present the time evolution of the relative distance d_{12} and the relative velocity v_{12} of the center of mass of the two fission fragments, respectively. The solid symbols denote the status after the scission point.

fm, it is found that the possibility of fission peaks at $b = 6$ fm. Since we are not to make quantitative comparison to experimental data, so in the whole discussions of this letter, only the calculations at $b = 6$ fm are concerned. Fig. 1 presents the evolution of two typical fission events. They are selected according to the mass asymmetry of the fission fragments. One is a near-symmetrical fission event ($A_1 = 95$, $A_2 = 105$, red open circles), and the other is an asymmetrical fission event ($A_1 = 46$, $A_2 = 156$, blue solid squares). In the process of fast fission, the definition of the fission fragments follows the reference [52]. Once the fission fragments are recognized after the scission point, the behavior of the nucleons belonging to the two fission fragments can be traced back to the very beginning of the collision, with $t = 0$ fm/c corresponding to the initial distance of 30 fm between the project and the target. The open symbols represent the status before the scission points in the two events.

Fig. 1 (a) presents the distance d_{12} of the center of mass of the two fission fragments as a function of time for the two fission events, with the solid symbols starting from the time when the fission fragments are recognized. The difference between the two events is evident. For the symmetrical fission case, the distance d_{12} of the fragments is close to 0 fm with $t < 500$ fm/c when the fission mode is not yet established. During the time from 500 fm/c to 1000 fm/c, d_{12} gradually shows an increasing trend with time, indicating further elongation of the TLF after its formation. After 1000 fm/c or so, R_{12} increases more rapidly as a result of the rapid separation of the fission fragments due to the Coulomb repulsion after the TLF ruptures completely. On the contrary to the symmetrical fission, in the asymmetrical fission event, the distance d_{12} between the two fragments increases rapidly right after the contact of the project and the target, showing significant dynamic effect and much faster elongating of the system.

Correspondingly the time evolution of the relative velocity of the two fragments is depicted in Fig. 1 (b). Consistently, for the symmetrical fission, the relative velocity v_{12} stays fair low because the colliding system undergoes strong dissipation before the fission channel is formed. Near 1000 fm/c when the fission fragments separate eventually, v_{12} increases constantly as a result of the Coulomb repulsion until it saturates at 2.4 cm/ns, which satisfies Viola systematics [57]. For the asymmetrical fission process, because of the dynamic feature carrying the memory of the incident channel, part of the projectile contributes directly to the light fission fragment and the elongation of the system is very fast. Hence its average velocity with respect to the heavy fragment is not fully dissipated before the two fragments rupture and the kinetic energy appears larger than the Viola systematics.

To investigate the effect of the neck formed in a dissipative elongation and the fast fission of the heavy TLF on the particle emission, in the following analysis, we will concentrate on the particle emission associated with the symmetrical fission events. We adopt the cut of $|\eta_a| < 0.2$ to select the symmetrical fission, where $\eta_a = \frac{A_1 - A_2}{A_1 + A_2}$ is the mass asymmetry of the fission fragments.

The splitting of the highly excited TLF is accompanied by the emission of light particles that carry isospin information depending sensitively on $E_{sym}(\rho)$. On the other hand, the source of light particles is rather complicated, originating from not only the fissioning TLF but also from all the stages of the colliding system regardless of whether fast fission occurs [40,43]. Thus, to see the effect of the fissioning TLF on the particle emissions, one has to compare the spectra of the light particles in the fast fission events with those in the events without undergoing fission. To overcome the commonly existing deficiency of clustering in transport models, we adopt the coalescence-invariant nucleons to represent the yield of light particles with $Z < 3$, where Z is the charge of the species. The coalescence-invariant neutron (CIN) and coalescence-invariant protons (CIP) yields are defined [56], respectively, as follows:

$$Y_{CIN} = \sum_i N_i Y_i(N, P) , \tag{5}$$

$$Y_{CIP} = \sum_i P_i Y_i(N, P) . \tag{6}$$

Here, the subscript i denotes the type of a certain light particle with $Z < 3$, and N_i (P_i) is the neutron (proton) number in the species i. Then the ratio of the CIN and CIP is defined as

$$R_{CINP} = Y_{CIN}/Y_{CIP} . \tag{7}$$

Fig. 2 present the average yield of CIN and CIP (a) and the emission rate (b), i.e., differential yield in a time interval of 200 fm/c, in two groups of events, with fast fission (solid symbols) and without fast fission (open symbols), respectively. The spurious emissions of CIN and CIP, as shown by the dashed curves in the panels, have been calculated over 100 events by setting the impact parameter $b = 30$ fm and subtracted to obtain the yield and the emission rate. It can be seen that the yield of CIN and CIP increases with time for both groups of events before 500 fm/c, which is roughly the fast fission time according to our simulations at this energy domain [52]. After the fast fission occurs, the yield of the CIN becomes increasingly enhanced in the event of fast fission while the yield of CIP exhibits an insignificant difference. It is consistent with the picture that starts with the formation of the neck, the fissioning TLF and the fission fragments tend to repel more neutrons, free or bounded in clusters, to the gas phase due to the density gradient of symmetry energy which drives neutrons and protons differently. The emission rate of CIN and CIP as a function of time is further presented in Fig. 2(b). A bump is visible before 500 fm/c on the emission rate distribution due to the high excitation energy enhancing the emission of particles, which is the same expectedly for those two categories of events with and without fission. After 500 fm/c, however, the occurrence of fast fission makes the emission of light particles significantly different. The emission of CIN is enhanced by about 25% lasting constantly to the final time while the emission of CIP shows insignificantly difference between the two groups of events with or without fast fission.

Fig. 3 presents the angular distribution of the emission rate of CIN (upper panels) and CIP (lower panels) in the center of mass

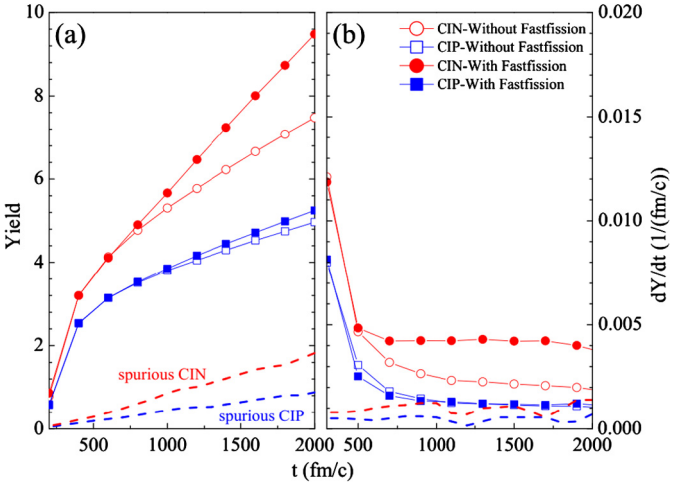

Fig. 2. The comparison of CIN (CIP) the emission between the events with (solid) and without (open) undergoing fast fission. Panel (a) presents the integrated yield while panel (b) presents the emission rate (dY/dt) with the time interval of 200 fm/c. In both panels, the open circle (square) represents the results of CIN (CIP) in the events without fission, and the solid circle (square) represents results of CIN (CIP) in the fast fission events.

at a different time for the events with (solid) and without (open) fast fission. Since the spurious emission has negligible effect on the ratio of $R_{\rm CINP}$, it is not considered in the following discussions. First, the following common feature can be seen for both CIP and CIN in both categories of events, at the earlier stage, the angular distribution shows asymmetric feature with peak situating at a forward angle due to the kinetic effect of the collisions, regardless of whether the fast fission follows. While at late stages, the relative contribution from the large angles increases and the angular distribution tends to become near symmetric with respect to $\theta_{\rm cm} = 90°$. Second, the emission rate of both CIN and CIP decreases with time because of the cooling of the system. Third, in accordance with the behavior in Fig. 2, the fast fission results in an enhancement in the emission of CIN, while the CIP is less impacted by the occurrence of the fission. And last, because the fission occurs at the time of hundreds fm/c, the enhancement of CIN emission is pronounced at large angles close to the rapidity of the TLF.

It should be mentioned here that in the process of fast fission, the yield of CIN and its angular distribution is not sensitive to the fine division of the mass asymmetry of the fission fragments, and this feature exists throughout the whole reaction process. The enhancement of the CIN yield in the fast fission events has possibly two origins. First, the total surface larger becomes larger when the TLF is separated in two smaller fragments possessing less neutron excess. As a result, more particles, particularly more neutrons are emitted from the surface, which is similar to the case of statistic fission [57]. A simple estimation shows that the surface is 20% larger in the fast fission events than in non-fission events and approximately accounts for the similar enhancement of the post-scission CIN yields. The variation of the mass asymmetry $\eta_{\rm a}$ brings less than 5% change of the total surface. However, it is worth mentioning that the surface area interpretation does not apply for CIP yield because of the interplay of the Coulomb barrier. Second, the presence of the fission neck favors the emission of neutrons for its low-density and neutron-rich feature. This can be testified experimentally by measuring the averagely enhanced neutron richness of the emissions perpendicular to the fission axis.

Next, we investigate the effects of $E_{\rm sym}(\rho)$ on CIN and CIP in fast fission events by comparing the simulations results at different $C_{\rm s}$ and γ_i, the $C_{\rm s}$ is varied in the range from 36 to 44 in a step of 2 MeV, corresponding to the value of $E_{\rm sym}(\rho)$ situating between 30.5 to 34.5 MeV at ρ_0, while the power coefficient γ_i is varied from 0.6 to 1.1, corresponding to the slope parameter L of $E_{\rm sym}(\rho)$ between 56 and 83 MeV in accordance with the rough constraints obtained from various observables. The results are presented in Fig. 4. In the upper panels (a)−(f) presented are the yields of the CIN (red solid) and CIP (blue open), respectively. From left to right, the results with $\gamma_i = 0.6$ to 1.1 are plotted. For a clear display, only the calculations with $C_{\rm s} = 36, 40$ and 44 are plotted. Correspondingly, the CI n/p ratios $R_{\rm CINP}$ are plotted in the lower panels (g)− (l).

Let us look at panels (a)−(f). First, the yield of CIN is generally larger than that of CIP in all situations. For the angular distribution, both CIN and CIP yields are more abundant in forward angles than in backward angles. From left to right, with the increase of γ_i, the emission of both CIN and CIP decreases. Careful survey to the $C_{\rm s}$ dependence reveals that more CIN particles are emitted with increasing the $C_{\rm s}$, whereas the CIP emission depends insignificantly on $C_{\rm s}$with an exception at small $\gamma_i = 0.6$ and 0.7 where CIP emissions increase with $C_{\rm s}$ too. The isospin observable $R_{\rm CINP}$ as a function of the angle $\theta_{\rm cm}$ in center of mass frame is then plotted in panels (g)−(l) in Fig. 4. In all cases, the ratios $R_{\rm CINP}$ exhibit an increasing trend with $\theta_{\rm cm}$. It suggests that the emitted light particles are averagely more neutron rich at large angles although the respective yields are low. The increasing trend is consistent with our earlier calculations in [56], but looks seemingly controversial against the experimental results in [42]. This is indeed because in later the free neutrons were not measured experimentally. Furthermore, at large angles with $\theta_{\rm cm} > 90°$, both the value and the increasing rate of $R_{\rm CINP}$ present a dependence γ_i which is more pronounced compared to that at forward angles with $\theta_{\rm cm} < 90°$. It suggests that $R_{\rm CINP}$ at large angles is potentially a sensitive probe of $E_{\rm sym}(\rho)$.

To extract the observable which is less influenced by the systematic numerical uncertainty of the transport model, we construct the double ratio of $R_{\rm CINP}$ in two angular windows $\theta_1 \pm 10°$ and $\theta_2 \pm 10°$ $(\theta_2 > \theta_1)$ by

$$DR_{21} = \frac{R_{\rm CINP}(\theta_2)}{R_{\rm CINP}(\theta_1)} . \tag{8}$$

For the forward (backward) region, we choose $\theta_1 = 30°(90°)$ and $\theta_2 = 90°(150°)$, respectively. The results are plotted in Fig. 5 (a) and (b), respectively. It is convincingly shown that the double ratios increase with γ_i evidently in both regions, while the dependence on $C_{\rm s}$ within the current range is rather marginal. More interestingly, the variation range of DR_{21} from $\gamma_i = 0.6$ to 1.1 is about 40% wider in the backward region than that in the forward region, indicating an enhanced sensitivity of DR_{21} on γ_i with $\theta_{\rm cm} \geq 90°$. It is consistent with the picture that the sensitivity of $R_{\rm CINP}$ depending on $E_{\rm sym}(\rho)$ is enhanced at large angles where more late-stage emissions are contributed and the isospin effect is accumulated. The comparisons confirm that the angular distribution of the $R_{\rm CINP}$, from which the double ratio DR_{21} can be extracted in fast fission events, is a sensitive probe to provide a further stringent constraint on the power coefficient γ_i (equivalently the slope parameter L) of $E_{\rm sym}(\rho)$ as a function of density.

It is currently known that the two parameters γ_i and $C_{\rm s}$ are correlated for many identified $E_{\rm sym}(\rho)$ probes. So the sensitive dependence of the isospin observable DR_{12} on γ_i, but not on $C_{\rm s}$ has an important experimental implication. Neutrons are the most important component in the CIN yield carrying the information of nuclear symmetry energy, even though the yields of nucleons in transport model simulations are usually overestimated. Due to the boost effect in the kinetics of a fixed target experiment, the neutrons at target rapidity (corresponding to large angles) have lower velocity and lower multiplicity. Both effects will bring advantages to the experimental measurement of neutrons, namely by improving the particle identification and suppressing multi hit ambiguity. In this regard, the enhanced $R_{\rm CINP}$ at large angles in the fission

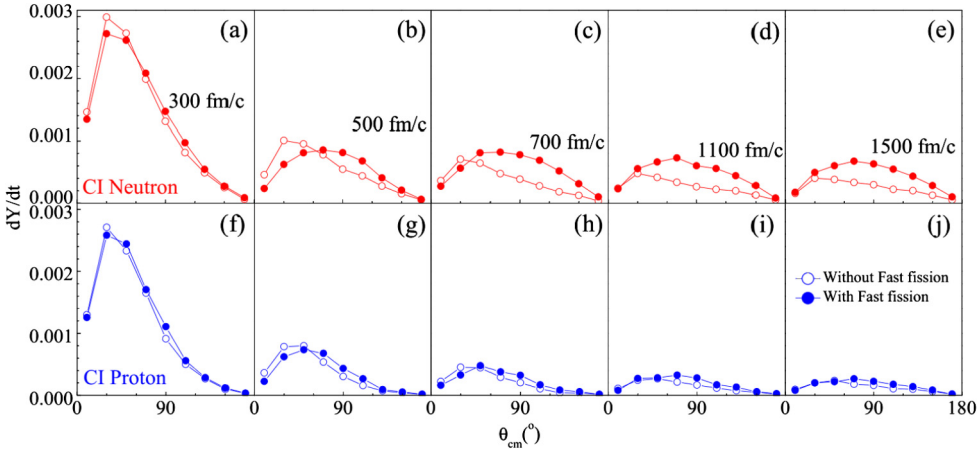

Fig. 3. The comparison of the angular distribution of emission rate for CIN and CIP at different time between fast fission events (solid) and non-fission events (open). Panels (a) – (f) represent the emission rate distribution of CIN while panels (g) – (l) are for the CIP.

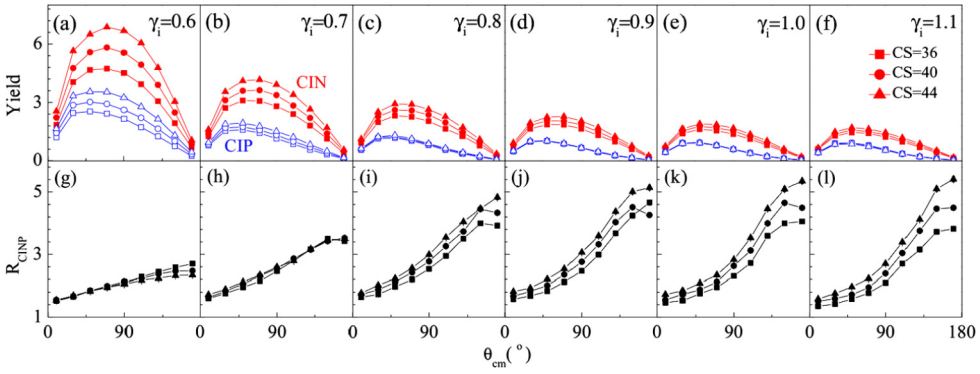

Fig. 4. The yield and ratio of CIN (red solid) and CIP (open blue) in fast fission events. Panels(a)–(f) are the angular distribution of CIN and CIP products for $\gamma_i = 0.6$ to 1.1 at $C_s = 36$ (square),40 (circle) and 44 (triangle), respectively. Panels (g)–(l) are the angular distributions of the CI n/p ratios R_{CINP}.

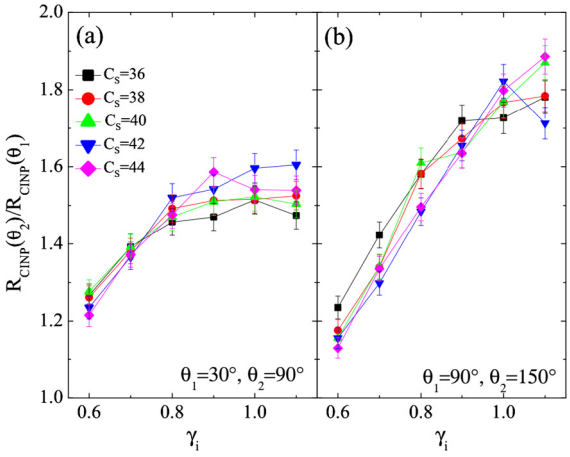

Fig. 5. The double ratio DR_{12} of the CI n/p R_{CINP} in the forward region (a) and backward region (b) as a function of γ_i with different C_s.

events can be used as a sensitive probe to the density dependence of $E_{sym}(\rho)$ near ρ_0 if experimental statistics suffices. Our findings are also consistent with the previous studies that light particles emitted in heavy ion reactions possess advantages to constrain the nuclear symmetry energy at low densities [58–61].

4. Summary

The emission of light particles in coincidence with the fast fission following the reaction ^{40}Ar+^{197}Au at 30 MeV/n ($b = 6$ fm) has been studied using the ImQMD model. The results show that the mass asymmetry of the fission fragments is correlated to the dissipation between the projectile and the target by means of momentum and nucleon exchange. Associated to the fast fission of the TLF, the CIN emissions are significantly enhanced due to the occurrence of the fission. The CI n/p ratio R_{CINP} as a function of angle in the center of mass depends sensitively on the power coefficient γ_i (equivalently the slope parameter L of $E_{sym}(\rho)$ on density) of the symmetry potential energy but marginally on the symmetry potential coefficient C_s. Because of the kinetic boost effect in the reactions on a fixed target, it is experimentally advantageous to measure the light particles including neutrons and protons at large angles, and the R_{CINP} ratio in coincidence with the fission fragments in heavy ion reactions at Fermi energies serves as a new and effective probe to constrain the nuclear symmetry energy at sub-saturation density.

Declaration of competing interest

I declare herewith that there are no conflicts of interest concerning our submission “Symmetry energy effect on emissions of light particles in coincidence with fast fission”.

Acknowledgements

This work is supported by the National Natural Science Foundation of China under Grant Nos. 11961131010, 11875174, 11890712, 11875323 and 11790320, by the Polish National Science Center under Grant No. 2018/30/Q/ST2/00185 and by Center of High Performance Computing, Tsinghua University. The authors thank Prof. Junlong Tian from ANU for his valuable discussions.

References

[1] B.P. Abbott, et al., Phys. Rev. Lett. 119 (2017) 161101.
[2] B.P. Abbott, et al., Phys. Rev. Lett. 121 (2018) 161101.
[3] S. De, D. Finstad, J.M. Lattimer, et al., Phys. Rev. Lett. 121 (2018) 091102.
[4] W.J. Xie, B.A. Li, Astrophys. J. 883 (2019) 174.
[5] Z.Y. Zhu, E.P. Zhou, A. Li, Astrophys. J. 862 (2018) 98.
[6] N.B. Zhang, B.A. Li, J. Xu, Astrophys. J. 859 (2018) 90.
[7] N.B. Zhang, B.A. Li, Eur. Phys. J. A 55 (2019) 39.
[8] M.B. Tsang, T.X. Liu, L. Shi, et al., Phys. Rev. Lett. 92 (2004) 062701.
[9] B.A. Li, C.B. Das, S.D. Gupta, et al., Nucl. Phys. A 735 (2004) 563.
[10] L.W. Chen, Che Ming Ko, Bao-An Li, Phys. Rev. Lett. 94 (2005) 032701.
[11] B.A. Li, C.M. Ko, Z. Ren, Phys. Rev. Lett. 78 (1997) 1644.
[12] M.A. Famiano, T. Liu, W.G. Lynch, et al., Phys. Rev. Lett. 97 (2006) 052701.
[13] M.B. Tsang, W.A. Friedman, C.K. Gelbke, et al., Phys. Rev. Lett. 86 (2001) 5023.
[14] L.W. Chen, C.M. Ko, B.A. Li, J. Xu, Phys. Rev. C 82 (2010) 024321.
[15] M.B. Tsang, Y. Zhang, P. Danielewicz, et al., Phys. Rev. Lett. 102 (2009) 122701.
[16] Y.G. Ma, G.H. Liu, X.Z. Cai, et al., Phys. Rev. C 85 (2012) 024618.
[17] L.W. Chen, V. Greco, C.M. Ko, B.A. Li, Phys. Rev. Lett. 90 (2003) 162701.
[18] M. Liu, N. Wang, Z.X. Li, F.S. Zhang, Phys. Rev. C 82 (2010) 064306.
[19] P. Russotto, S. Gannon, S. Kupny, et al., Phys. Rev. C 94 (2016) 034608.
[20] Y. Zhang, M. Liu, C.J. Xia, et al., Phys. Rev. C 101 (2020) 034303.
[21] B.A. Li, L.W. Chen, C.M. Ko, Phys. Rep. 464 (2008) 113.
[22] Z.G. Xiao, G.C. Yong, L.W. Chen, et al., Eur. Phys. J. A 50 (2014) 37.
[23] J. Xu, Prog. Part. Nucl. Phys. 106 (2019) 312.
[24] P. Morfouace, C.Y. Tsang, Y. Zhang, et al., Phys. Lett. B 799 (2019) 135045.
[25] Y. Zhang, M.B. Tsang, Z. Li, Phys. Lett. B 749 (2015) 262.
[26] J. Xu, L.W. Chen, M.Y.B. Tsang, et al., Phys. Rev. C 93 (2016) 044609.
[27] M. Colonna, et al., Eur. Phys. J. A 50 (2014) 30.
[28] L. Ou, Z. Xiao, H. Yi, et al., Phys. Rev. Lett. 115 (2015) 212501.
[29] X. Liang, L. Ou, Z.G. Xiao, Phys. Rev. C 101 (2020) 024603.
[30] P. Glässel, D. Harrach, H.J. Specht, et al., Z. Phys. A 310 (1983) 189.
[31] S. Leray, X.S. Chen, G.Y. Fan, et al., Nucl. Phys. A 423 (1984) 175.
[32] Z. Zheng, B. Borderie, D. Gards, et al., Nucl. Phys. A 422 (1984) 447.
[33] A.A. Stefanini, G. Casini, P.R. Maurenzig, et al., Z. Phys. A 351 (1995) 167.
[34] R. Vandenbosch, K.L. Wolf, J. Unik, et al., Phys. Rev. Lett. 19 (1967) 1138.
[35] I.I. Gontchar, R.A. Kuzyakin, Phys. Rev. C 84 (2011) 014617.
[36] M. Kaur, M.K. Sharma, R.K. Gupta, et al., Phys. Rev. C 86 (2012) 064610.
[37] S. Hudan, A.B. McIntosh, R.T. De Souza, et al., Phys. Rev. C 86 (2012) 021603(R).
[38] V. Baran, M. Colonna, M. Di Toro, Nucl. Phys. A 730 (2004) 329.
[39] V.E. Viola Jr, G.T. Seaborg, J. Inorg. Nucl. Chem. 28 (1966) 741.
[40] F. Benrachi, B. Chambon, B. Cheynis, et al., Phys. Rev. C 48 (1993) 2340.
[41] D.J. Hinde, H. Ogata, Phys. Rev. C 39 (1989) 2268.
[42] Y. Zhang, J. Tian, W. Cheng, et al., Phys. Rev. C 95 (2017) 041602R.
[43] R.S. Wang, Y. Zhang, Z.G. Xiao, et al., Phys. Rev. C 89 (2014) 064613.
[44] L.G. Sobotka, Phys. Rev. C 50 (1994) 1272(R).
[45] E. De Filippo, A. Pagano, P. Russotto, et al., Phys. Rev. C 86 (2012) 014610.
[46] A. Jedele, A.B. McIntosh, K. Hagel, et al., Phys. Rev. Lett. 118 (2017) 062501.
[47] N. Le Neindre, M. Alderighi, A. Anzalone, et al., Nucl. Instrum. Methods A 490 (2002) 251.
[48] J. Pouthas, B. Borderie, R. Dayras, et al., Nucl. Instrum. Methods A 357 (1995) 418.
[49] O. Lopez, et al., Nucl. Instrum. Methods A 884 (2018) 140.
[50] S. Wuenschel, et al., Nucl. Instrum. Methods A 604 (2009) 578.
[51] M.S. Wallace, et al., Nucl. Instrum. Methods A 583 (2007) 302.
[52] Q.H. Wu, X.Y. Diao, et al., Phys. Lett. B 797 (2019) 134808.
[53] V. Zanganeh, N. Wang, O.N. Ghodsi, Phys. Rev. C 85 (2012) 034601.
[54] N. Wang, L. Ou, Y. Zhang, Z. Li, Phys. Rev. C 89 (2014) 064601.
[55] C. Li, J. Tian, L. Ou, N. Wang, Phys. Rev. C 87 (2013) 064615.
[56] Q.H. Wu, Y.X. Zhang, Z.G. Xiao, et al., Phys. Rev. C 91 (2015) 014617.
[57] K. Pomorski, B. Nerlo-Pomorska, M. Warda, et al., Nucl. Theory 36 (2017).
[58] V. Baran, M. Colonna, M. Di Toro, et al., Phys. Rev. C 72 (2005) 064620.
[59] Z.Q. Feng, Phys. Rev. C 94 (2016) 014609.
[60] Y. Zhang, C. Zhou, J. Chen, et al., Sci. China, Phys. Mech. Astron. 58 (2015) 112002.
[61] M. Kaur, S. Gautam, R.K. Puri, Nucl. Phys. A 955 (2016) 133.